Published in final edited form as:
Mol Cell Neurosci. 2011 March ; 46(3): 655–661. doi:10.1016/j.mcn.2011.01.005.

Missense mutations in Otopetrin 1 affect subcellular localization and inhibition of purinergic signaling in vestibular supporting cells

Euysoo Kim[1], **Krzysztof L. Hyrc**[2], **Judith Speck**[3], **Felipe T. Salles**[4], **Yunxia W. Lundberg**[5], **Mark P. Goldberg**[6], **Bechara Kachar**[4], **Mark E. Warchol**[3], and **David M. Ornitz**[1]

[1]Department of Developmental Biology, Washington University School of Medicine, Saint Louis, Missouri 63110

[2]Department of Neurology, Washington University School of Medicine, Saint Louis, Missouri 63110

[3]Department of Otolaryngology, Washington University School of Medicine, Saint Louis, Missouri 63110

[4]Laboratory of Cell Structure and Dynamics, National Institute of Deafness and Other Communication Disorders, National Institutes of Health, Bethesda, Maryland 20892

[5]Department of Genetics, Boys Town National Research Hospital, Omaha, Nebraska 68131

[6]Department of Neurology, University of Texas Southwestern Medical Center, Dallas, Texas 75390

Abstract

Otopetrin 1 (*Otop1*) encodes a protein that is essential for development of otoconia. Otoconia are the extracellular calcium carbonate containing crystals that are important for vestibular mechanosensory transduction of linear motion and gravity. There are two mutant alleles of *Otop1* in mice, *titled* (*tlt*) and *mergulhador* (*mlh*), which result in non-syndromic otoconia agenesis and a consequent balance defect. Biochemically, Otop1 has been shown to modulate purinergic control of intracellular calcium in vestibular supporting cells, which could be one of the mechanisms by which Otop1 participates in the mineralization of otoconia. To understand how *tlt* and *mlh* mutations affect the biochemical function of Otop1, we examined the purinergic response of COS7 cells expressing mutant Otop1 proteins, and dissociated sensory epithelial cells from *tlt* and *mlh* mice. We also examined the subcellular localization of Otop1 in whole sensory epithelia from *tlt* and *mlh* mice. Here we show that *tlt* and *mlh* mutations uncouple Otop1 from inhibition of P2Y receptor function. Although the *in vitro* biochemical function of the Otop1 mutant proteins is normal, *in vivo* they behave as null alleles. We show that in supporting cells the apical membrane localization of the mutant Otop1 proteins is lost. These data suggest that the *tlt* and *mlh* mutations primarily affect the localization of Otop1, which interferes with its ability to interact with other proteins that are important for its cellular and biochemical function.

Corresponding author David M. Ornitz Washington University School of Medicine, Department of Developmental Biology Campus Box 8103, 660 S. Euclid Avenue, Saint Louis, MO 63110 USA Tel: 314-362-3908 Fax: 314-362-7058 dornitz@wustl.edu .

Keywords

vestibular; otoconia; Otopetrin; calcium; purinergic signaling

1. Introduction

Otopetrin 1 (*Otop1*) is the founding member of a gene family that is conserved in all vertebrates (Hughes et al., 2008; Hurle et al., 2003). Otop1 is predicted to be a twelve transmembrane (TM) domain protein, containing three phylogenetically conserved Otopetrin Domains (ODI, ODII, ODIII) (Hughes et al., 2008). ODs lack homology to any known functional domain, but retain homology to sequences found in arthropods and nematodes (Hughes et al., 2008). A function of Otop1 was first revealed by studying the phenotype of mice containing two different missense mutations in the *Otop1* gene leading to non-conservative amino acid substitutions (Hurle et al., 2003). The first mutation, *tilted* (*tlt*), is a spontaneous mutation (Ala_{151}->Glu in TM3) which is maintained on the C57BL/6J background (Lane, 1986; Ornitz et al., 1998). *Mergulhador* (*mlh*) is a mutation in *Otop1* (Leu408->Gln in TM9) that arose in an ENU mutagenesis screen in a BALB/cJ genetic background (Massironi et al., 1994). Both *tlt* and *mlh* homozygous mice lack a perception of gravity and linear motion due to non-syndromic agenesis of both utricular and saccular otoconia. The resulting deficits in balance have a penetrance approaching 100 percent.

Otoconia are calcium carbonate crystals localized in extracellular clusters above the sensory epithelia (macula) of the utricle and saccule in the inner ear. Each crystal is composed of a proteinaceous core surrounded by a shell composed of $CaCO_3$ micro-crystals in the form of calcite (Mann et al., 1983). Otoconia are on average three times denser than the fluid (endolymph) that bathe them, and this characteristic allows them to precisely enhance an organism's sensitivity to linear motion (Carlstrom et al., 1953; Grant and Best, 1987). Resulting movement of otoconia deflects the underlying stereocilia of the hair cells in the sensory epithelium, leading to depolarization of the hair cells and propagation of electrical signals to the brain.

Recent studies suggest a function for Otop1 in the calcification of otoconia. Otop1 expression in heterologous cells (Hughes et al., 2007) and targeted inactivation of endogenous Otop1 in mouse utricular epithelial cultures (Kim et al., 2010) demonstrate a role for Otop1 in the modulation of purinergic (P2) signaling mediated by ligands such as ATP. In the presence of Otop1, P2Y receptor-mediated Ca^{2+} release from intracellular stores was inhibited, whereas P2X receptor-like influx of Ca^{2+} was induced. These studies showed that Otop1 can modulate intracellular Ca^{2+} concentrations ($[Ca^{2+}]_i$) both *in vitro* and *in vivo*. Importantly, the kinetics and characteristic of modulation of $[Ca^{2+}]_i$ by Otop1 resembled ATP-mediated increases in intravesicular $[Ca^{2+}]$ observed in isolated globular substance vesicles (putative precursors of otoconia) (Suzuki et al., 1997). This suggested that Otop1 could be the endogenous protein that regulates globular substance vesicle $[Ca^{2+}]$ to induce calcification of otoconia.

Of primary importance to understanding how Otop1 functions in the biosynthesis of otoconia is to understand the mechanism(s) by which Otop1 function is altered or disrupted by mutations that result in failure to form otoconia. *Tlt* and *mlh* mutations, found within transmembrane domains of Otop1, are predicted to alter the hydrophobicity of the transmembrane domains, which may alter protein topology, folding, trafficking, and/or biochemical activity. In this study, we examined how *tlt* and *mlh* mutations affected subcellular localization of Otop1 and the ability of Otop1 to modulate purinergic signaling both *in vitro* and *in vivo* using a transient transfection system and mouse organ culture

explants. We show that *tlt* and *mlh* mutations do not interfere with the ability of Otop1 to inhibit P2Y receptor signaling, but rather alter the subcellular localization of Otop1 in the macular epithelium. This observation emphasizes the importance of apical trafficking and/or localization of Otop1 near the apical membrane of supporting cells, and suggests that Otop1 may interact with other proteins localized at or near the apical membrane or regulate the formation or composition of vesicles (globular substance) released by the sensory supporting cells.

2. Materials and Methods

2.1. Construction of Otop1^{tlt} and Otop1^{mlh} expression vectors

EGFP-Otop1 was constructed as previously described (Hughes et al., 2007), where the full length cDNA clone of *Otopetrin 1* (A530025J20, obtained from RIKEN Laboratories) was ligated into the pCS2EGFP vector. The pCS2EGFP empty vector was used as a cytosolic EGFP control. To construct *Otop1^{tlt}* (Ala_{151}-> Glu) and *Otop1^{mlh}* (Leu_{408}-> Gln) expression vectors, PCR-based site-directed mutagenesis was performed to induce these mutations in *EGFP-Otop1* constructs. Primers used to induce *tlt* and *mlh* mutations were as follows: *tlt*, primer 1 (5′- ATGAAGTATTCGACTTTCAAGCATCCCAGGACG -3′ (reverse)), *tlt*, primer 2 (5′- AAAGTCGAATACTTCATTGGATTCTCGGAGTGC -3′ (forward)), *mlh*, primer 1 (5′- ATGGCCTGAATGGAGCCCCAGGAGAGG -3′ (reverse)), *mlh*, primer 2 (5′- TCCATTCAGGCCATCGCCTGTGCTGAG -3′ (forward)).

PCR conditions: 25 cycles of denaturation at 94°C for 1 min, annealing at 63°C for 1 min, and extension at 72°C for 2 min.

2.2. Cell culture and transfection

COS7 cells were maintained in growth media, containing Dulbecco's Modified Eagle's Medium (Invitrogen, Carlsbad, CA) supplemented with 10% fetal calf serum (Invitrogen, Carlsbad, CA), 2mM L-glutamine, and 1X penicillin/streptomycin. Cells were plated on 35 mm plates with glass coverslips (MatTek Corporation, Ashland, MA) for 24-48 hours before transfection. Cells were transfected using Lipofectamine 2000 (Invitrogen, Carlsbad, CA) and approximately 1 μg plasmid DNA in OptiMEM (Invitrogen, Carlsbad, CA) for 4-5 hours following manufacturer's instructions. Cultures were allowed to recover overnight in growth media and then were used for ratiometric calcium imaging experiment.

2.3. Mice

Mlh mice were maintained on a BALB/cJ genetic background. The *mlh* allele was genotyped using PCR primers, 5′-TGAGAAGTCTCTGGATGAGTC (forward) and 5′-GAATAACAACAGCTTGATGAA G (reverse) to amplify a 542 bp fragment, followed by restriction enzyme digestion to detect loss of an MscI restriction site in the *Otop1^{mlh}* allele (Hurle et al., 2003).

Tlt mice were maintained on a C57BL/6J genetic background. The *tlt* allele was genotyped using PCR primers, 5′-CACTGTTTGGTCTTGGTACC (forward) and 5′-CAGCTCATTATTCCTGACAAG (reverse) to amplify a 391 bp fragment, followed by restriction enzyme digestion to detect gain of a TaqI restriction site in the *Otop1^{tlt}* allele (Hurle et al., 2003).

The *Otop1$^{\beta gal}$* allele (Kim et al., 2010) was genotyped with the following primers: primer 1 (5′-AGGGTCTCCACAAGCTTCCGGT-3′ (forward)); primer 2 (5′-TGACAGCCTACAGCCCAGGATG-3′ (*Otop1$^{+/+}$* reverse)); primer 3 (5′-

CCATTCAGGCTGCGCAACTGT-3′ (*Otop1*$^{\beta gal}$ reverse)). The wild type allele amplifies a 545 bp fragment and the targeted allele amplifies a 369 bp fragment.

2.4. Preparation of mouse utricular macular dissociated cultures

Utricles from E18.5 to P3 pups were dissected in Medium 199 (#12350039, Invitrogen, Calrsbad, CA), and the nonsensory epithelium and otoconial layer were completely removed. Tissues were then incubated in thermolysin (Sigma, St. Louis, MO) (500 μg/ml in Medium 199) at 37°C for 50 min, and the isolated epithelial sheets were further treated with Trypsin/EDTA (0.05%, 0.02%) for 15 min at 37 °C. After replacing Trypsin/EDTA with Medium 199, cells were triturated 5 to 10 times, plated on laminin coated MatTek dishes (MatTeck Corporation, Ashland, MA), and incubated overnight at 37°C. Medium 199 containing 10% fetal bovine serum (Invitrogen, Calrsbad, CA) was added the next day. The cells were cultured for an additional 24 hr prior to imaging.

2.5. Ratiometric calcium imaging and data analysis

All imaging experiments were carried out at room temperature in a HEPES-buffered salt solution (HCSS) containing, in mM: 140 NaCl, 5.4 KCl, 1 NaH_2PO_4, 1.8 $CaCl_2$, 1 $MgSO_4$, 12 HEPES, and 5.5 D-glucose, pH 7.4±0.1. COS7 cells or dissociated utricular macular cultures were loaded with fura-2 by incubation for 60 min with 5-10 μM acetoxymethyl (AM) ester (Invitrogen, Carlsbad, CA) and 0.1% Pluronic F-127 (Invitrogen, Carlsbad, CA) in HCSS (pH=7.2) at room temperature, washed with HCSS and incubated for another 60 min to allow for ester hydrolysis. After loading, cells were imaged on an inverted microscope (Nikon Eclipse TE300, Nikon Inc., Melville, NY) equipped with a cooled CCD camera (Cooke Corp., Auburn Hill, MI) using a 20x/0.45 Plan Fluor objective (Nikon). The fluorescence excitation (75 W xenon arc lamp) was provided by band-specific filters (340 and 380 nm; Semrock, Rochester, NY) in combination with a XF73 dichroic beam splitter (Omega Optical, Brattleboro, VA). Pairs of images were collected constantly at alternate excitation wavelengths. After subtracting the matching background, the image intensities were divided by one another to yield ratio values for individual cells.

For COS7 cells, fluorescent intensities of GFP (485 nm) and fura-2 (340 and 380 nm) channels were recorded. Analysis of fura-2 signal intensities in unloaded GFP-expressing cells showed that approximately 4% and 23% of the GFP signal bleeds through 340 and 380 fura-2 channels, respectively. Therefore, the signal intensity contributed by the presence of GFP was subtracted from fura-2 fluorescence for each cell before calculating indicator ratio. 100 μM ATP (Sigma, St. Louis, MO) was used for all ratiometric calcium analysis. For studies done with mouse macular dissociated cultures, 10 μM ionomycin (Calbiochem, San Diego, CA) was added at the end of each experiment to obtain the maximum level of $[Ca^{2+}]_i$ in each region of interest. To make data points comparable between experiments performed on different days, fura-2 ratio values in individual regions of interest were normalized as follows: Normalized Ratio = $(R-R_0)/(R_{max}- R_0)$, where R is the individual ratio value, R_{max} is the peak ratio after addition of ionomycin, R_0 is the average of the prestimulation baseline ratio.

2.6. Whole mount immunohistochemistry

Temporal bones were isolated in Leibovitz's medium L15 (Sigma, St. Louis, MO) and fixed in 4% paraformaldehyde for 1-2hr at RT. Utricular and saccular maculae were dissected from the temporal bones in cold PBS, incubated in 0.5% Triton X-100 for 30 min at room temperature, and then washed with PBS. Samples were blocked using 4% BSA/PBS overnight at 4°C, and incubated with rabbit anti-Otop1 antibody (1:800) for 90 min at room temperature in a humidified chamber. After washing with PBS, samples were incubated with secondary antibodies, Alexa 488 anti-rabbit IgG (1:600, Invitrogen, Carlsbad, CA) for 45

min at room temperature. For stereocilia staining, samples were further incubated with rhodamine-phalloidin (1:200, Invitrogen, Carlsbad, CA) for 15 min at room temperature. After washing with PBS, samples were transferred to a superfrost slide, mounted with vectashield (Vector Laboratories, Burlingame, CA), and coverslipped before imaging with an Olympus FV500a multi-channel confocal microscope (objective: 60X water, resolution: 512 × 512, average number of slices per stack: 125, thickness of each slice: 0.2 μm, average thickness of a stack: 25 μm). Analysis of pixel intensity with respect to the distance from the apical to basal plane of the sensory epithelium was done using Image J software (http://rsb.info.nih.gov/ij/). To obtain normalized pixel intensity values, each point was divided by the maximum value of each curve.

2.7. Overexpression of EGFP-Otop1, EGFP-Otop1^{tlt}, EGFP-Otop1^{mlh} in utricular culture cells using genegun transfection

Pieces of the whole utricular maculae were dissected from postnatal day 0–4 rats and attached to coverslips previously coated with Cell-Tak (150 μg/μL; BD Biosciences, San Jose, CA). Cultures were maintained in DMEM/F12 (Invitrogen, Carlsbad, CA) with 5–7% fetal bovine serum (FBS) and ampicillin (1.5 μg/mL; Sigma, St. Louis, MO) and maintained at 37 °C and 5% CO_2. For transfections, 50 μg of each expression vector was precipitated onto 25 mg of 1 μm gold particles and loaded into Helios Gene Gun cartridges (BioRad, Hercules, CA). Tissue explants were transfected with the gene gun set at 95 psi of helium and maintained in culture for 24 hrs. The efficiency of gene gun transfection was approximately 5%.

2.8. Immunohistochemistry after transfection

Dissected tissue was fixed in 4% paraformaldehyde/PBS for 30 minutes. After washing with PBS, tissues were permeabilized with 0.5% Triton X-100/PBS and Alexa 568 phalloidin (1:200) (Invitrogen, Carlsbad, CA) for 30 minutes. Samples were blocked in 4% BSA/PBS for 2 hours, and then incubated with mouse monoclonal anti ZO-1 antibody (1:600) (Zymed, San Francisco, CA) for 60 minutes. For secondary detection, samples were incubated with goat anti-mouse Alexa 488 (Invitrogen, Carlsbad, CA). After washing with PBS, tissues were mounted onto glass slides with Prolong antifade gold reagent (Invitrogen, Carlsbad, CA). Imaging was done on a PerkinElmer Nikon Eclipse confocal microscope (100X 1.4 NA objective) and Volocity acquisition software (Perkin Elmer, Waltham, MA). Each optical section was 0.5 μm thick with a resolution of 0.05 μm/pixel. Three-dimensional rendering was made using Volocity 5.3.2 (Improvision, Coventry, UK).

3. Results

3.1. Tlt and mlh mutations do not affect Otop1 modulation of the purinergic response in vitro

Previously, COS7 cells overexpressing *EGFP*-tagged *Otop1* (*EGFP-Otop1*) were shown to modulate changes in the concentration of intracellular calcium ($[Ca^{2+}]_i$) in response to purinergic signals, such as ATP (Hughes et al., 2007). Pharmacological analysis showed that activation of P2Y receptors, which results in release of Ca^{2+} from IP_3-sensitive intracellular stores, is denoted by the initial peak, whereas influx of extracellular Ca^{2+} by P2X receptor activation is depicted in the following plateau phase (Hughes et al., 2007). In untransfected (WT) or *EGFP*-transfected COS7 cells, change in $[Ca^{2+}]_i$ in response to ATP was characterized by an increase in $[Ca^{2+}]_i$, forming a peak, followed by a lower but sustained increased in $[Ca^{2+}]_i$ (Fig. 1D). Consistent with previous studies, overexpression of *EGFP-Otop1* resulted in a change in how COS7 cells respond to 100 μM ATP; the initial peak in $[Ca^{2+}]_i$ was dramatically reduced and the increase in $[Ca^{2+}]_i$ resulted in a sustained plateau phase until wash (Fig. 1A). EGFP-Otop1 localizes to endoplasmic reticulum (ER), golgi,

and plasma membrane (PM) in COS7 cells (data not shown), but only protein localized in the PM is thought to mediate the purinergic signaling response (Hughes et al., 2007). Interestingly, the *tlt* and *mlh* mutations did not disrupt the subcellular localization of EGFP-Otop1 (data not shown) nor the ability of EGFP-Otop1 to modulate a purinergic response (Fig. 1A-C). Statistical analysis of the calcium response showed that overexpression of either the wild type or mutant forms of *EGFP-Otop1* accounted for ~80% decrease in the initial peak value (Fig. 1E). These data suggested that *tlt* and *mlh* mutations do not disrupt the domain(s) of Otop1 required for modulating purinergic receptors and intracellular $[Ca^{2+}]_i$.

3.2. Otop1-specific modulation of intracellular calcium is disrupted in primary cultures of utricular epithelial cells from tlt and mlh mice

The observation that *EGFP-Otop1*, *EGFP-Otop1*^{tlt} and *EGFP-Otop1*^{mlh}-expressing cells responded similarly to ATP suggested that these mutations might be interfering with other biochemical functions of Otop1. However, it was also possible that overexpression of a multi-transmembrane domain protein could cause unexpected effects on intracellular Ca^{2+} modulation and might not represent *in vivo* activity at normal levels of expression. Therefore, to determine whether endogenous Otop1^{TLT} or Otop1^{MLH} can alter the *in vivo* function of Otop1 in modulating purinergic signaling, dissociated macular supporting cell cultures from *Otop1*$^{+/+}$, *Otop1*$^{\beta gal/\beta gal}$ (*Otop1* knockout mice with an inserted β-galactosidase cDNA) (Kim et al., 2010), *Otop1*$^{tlt/tlt}$, and *Otop1*$^{mlh/mlh}$ inner ears were exposed to 100 μM ATP. In the *Otop1*$^{+/+}$ samples, addition of ATP resulted in an increase in $[Ca^{2+}]_i$, characterized by an elevated plateau that persisted until removal of the agonist (Fig. 2A, dotted line). Consistent with previous observations (Kim et al., 2010), in *Otop1*$^{\beta gal/\beta gal}$ maculae, the response to ATP showed a higher peak, followed by a reduction in $[Ca^{2+}]_i$ to an elevated plateau (Fig. 2A). The plateau level in *Otop1*$^{\beta gal/\beta gal}$ cells are slightly higher than that in *Otop1*$^{+/+}$ cells probably due to the higher initial peak values. Our previous study with mouse utricular macular epithelial cells showed that, like in COS7 cells, the initial peak results from Ca^{2+} release from intracellular stores (P2Y receptor function) and the plateau phase resulted from influx of extracellular Ca^{2+} (P2X receptor-like function) (Burnstock, 2007; Kim et al., 2010; North, 2002). Therefore, the different response to ATP in *Otop1*$^{+/+}$ and *Otop1*$^{\beta gal/\beta gal}$ cultures suggested that endogenous Otop1 functions to inhibit P2Y receptor function and induce an influx of extracellular Ca^{2+} *in vivo*.

Unlike what was observed in COS7 cells, *Otop1*$^{tlt/tlt}$ and *Otop1*$^{mlh/mlh}$ cultures showed a similar response to *Otop1*$^{\beta gal/\beta gal}$ cultures, with distinctly higher peak values (highest point after addition of ATP) compared to that of the *Otop1*$^{+/+}$ cultures (Fig. 2B-D). This indicated that Otop1-specific modulation of $[Ca^{2+}]_i$ is disrupted in mutant sensory epithelial cells. Importantly, epithelial cultures from heterozygous *tlt* or *mlh* mice (*Otop1*$^{tlt/+}$ and *Otop1*$^{mlh/+}$) showed a similar response to ATP to that observed in *Otop1*$^{+/+}$ cultures (Fig. 2E, F). This demonstrated that the mutations are unlikely to have dominant negative effects on Otop1 function and is consistent with the presence of normal otoconia in the heterozygous mutant mice and with the recessive genetics of the *tlt* and *mlh* mutations (Ornitz et al., 1998).

3.3. Tlt and mlh mutations affect localization and/or trafficking of endogenous Otop1

Tlt and *mlh* mutations are found in the predicted TM3 and TM9, respectively (Fig. 3A). Interestingly, TM3 and TM9 are localized in different Otopetrin Domains (ODs), suggesting that they could have distinct consequences on Otop1 function. To test whether these mutations could affect the subcellular localization of Otop1, we examined Otop1 protein localization using whole mount immunohistochemistry. The epitope for the anti-Otop1 antibody is located at the N-terminus of the protein before the first predicted TM (Fig. 3A,

red line). The predicted structure of Otop1 (Hughes et al., 2008), places this epitope on the cytosolic amino terminus of the Otop1 protein. Using confocal imaging and three-dimensional reconstruction we obtained XZ plane images of stained utricles (compressed in the y-axis, Fig. 3B-E) and saccules (data not shown) with which we could determine the relative apical - basal position of the Otop1 signal. As we obtained similar results for utricles and saccules, only data with the utricles are shown.

In *Otop1*$^{+/+}$ utricle, immunofluorescence signals were in a punctate pattern, located near the apical end of the sensory epithelium (Fig. 3B, G). The punctate pattern could result from protein localization on intracellular vesicles, owing to the multi TM domain structure of the protein (Fig. 3A,). Almost no signal was detected below the mid region of the epithelium (Fig. 3F). Because *Otop1*$^{\beta gal}$ allele still expresses the first two TM domains we were able to detect the localization of the β-galactosidase (βgal) fusion protein using our Otop1-specific antibody. Signal intensity in *Otop1*$^{\beta gal/\beta gal}$ tissue was greatly increased (Fig. 3C), and overall signals were localized at the mid region of the epithelium (Fig. 3F). This suggested that the fusion proteins formed aggregates within intracellular vesicles and could no longer be trafficked near the apical side of the epithelium. In *Otop1*$^{tlt/tlt}$ (Fig. 3D) and *Otop1*$^{mlh/mlh}$ (Fig. 3E) tissue, the signal clearly showed mislocalization of the mutant proteins. The signals were spread throughout the epithelium in a punctate pattern, and in most cells, very little signal was detected near the apical epithelium (Fig. 3F). Interestingly, the Otop1^{MLH} protein was localized more towards the basal epithelium than the Otop^{TLT} protein (Fig. 3D-F).

To confirm that the mislocalization of the mutant proteins is not due to altered development, but rather homeostatic localization of Otop 1 protein, we overexpressed *EGFP-Otop1*, -*Otop1*^{tlt}, and -*Otop1*^{mlh} in rat utricular maculae and examined the localization of GFP in transfected supporting cells. EGFP-Otop1 was found at a level comparable to Zona Ocluden-1 (ZO-1) and phalloidin signals, which marks the tight junction and the circumferential actin belt at the apical membrane , respectively (Fig 4A). We rarely observed signals below the apical membrane in transfected supporting cells because only the highest concentration of EGFP-Otop1 is visualized in the overexpression system. Consistent with what was observed *in vivo*, mislocalization of EGFP-Otop1^{TLT} and EGFP-Otop1^{MLH} was apparent. Most of the EGFP-Otop1^{TLT} protein was localized in the apical half of the cell body and only a small proportion was observed in the apical membrane of transfected supporting cells (Fig. 4B). The EGFP-Otop1^{Mlh} protein was similarly localized within the apical half of the cell body (Fig. 4C). These results suggested that the *tlt* and *mlh* mutations function to alter the localization of Otop1, and that apical membrane localization of Otop1 may be important for development of otoconia.

4. Discussion

Tlt and *mlh* are recessive alleles of *Otop1* that result in otoconia agenesis. Previous studies found that Otop1 can modulate intracellular calcium by inhibiting P2Y receptor signaling in response to ATP (Hughes et al., 2007; Kim et al., 2010). In this study, we sought to better understand the role of Otop1 by investigating the mechanism by which *tlt* and *mlh* mutations affect the function of Otop1.

To test the known biochemical activities of Otop1, we transiently expressed wild type and mutant alleles of *Otop1* in COS7 cells and performed ratiometric calcium imaging. Surprisingly, Otop1^{TLT} and Otop1^{MLH} showed no difference from wild type Otop1 in the ability to inhibit P2Y receptor function *in vitro*. This finding suggested that the inhibitory function of Otop1 on purinergic signaling may not be important for otoconia formation, that overexpression of Otop1 alleles masked differences in the biochemical function of wild type

and mutant proteins, or that COS7 cells may have different requirements for the regulation of purinergic signaling compared to sensory supporting cells.

To ensure that this result is not caused by complications of the overexpression system, we compared the activity of endogenous alleles of wild type and mutant Otop1 in explants of mouse utricular sensory epithelia. Importantly, the purinergic response of cultures derived from homozygous *tlt* and *mlh* mice were identical to that from homozygous *Otop1* knockout mice (*Otop1*$^{\beta gal/\beta gal}$), suggesting that these mutations in *Otop1* act as functional null alleles *in vivo*. This result, and the lack of a biochemical phenotype *in vitro*, suggested that the mutations might not be affecting the function of Otop1 to regulate purinergic signaling *per se* but that other factors critical for the protein's function, such as subcellular localization might be affected.

We therefore examined the subcellular localization of the wild type and mutant proteins in whole macular epithelia. Unlike the wildtype Otop1, Otop1^{TLT} and Otop1^{MLH} proteins did not localize to the apical surface of supporting cells. However, *in vitro*, since low levels of Otop1 protein are sufficient to inhibit P2Y signaling (Hughes et al., 2007), we posit that overexpression of Otop1^{TLT} and Otop1^{MLH} proteins in COS7 cells can overcome the defects caused by the mutations and place enough protein on the cell surface to impart maximal biochemical activity.

Our result that the mutant proteins change the localization of Otop1 suggests two possible mechanisms by which the mutations affect the protein; Mis-trafficking by interfering with functional domains; and/or mis-folding, which can be caused by a change in the hydrophobicity of a protein (Dobson, 2003). Because there was no major difference in fluorescent intensity of endogenous or overexpressed Otop1 signals in the wildtype or mutant samples, we can provisionally rule out the possibility that the mutations cause protein degradation due to misfolding. However, a quantitative analysis of protein levels by Western Blot will more accurately address this issue.

Expression of *EGFP-Otop1* in MDCK cells did not show localization towards the apical region (data not shown), suggesting that the apical localization of Otop1 is specific and may be dependent on proteins specific to the macular epithelium. Future studies will be needed to examine whether Otopetrin Domains are important for interaction with macular-specific proteins and proper targeting of Otop1.

Requirement of apical targeting for regulation of purinergic signaling suggests a possible interaction of Otop1 with an ATP responsive protein or ATP itself. The prominent Otop1 signal beneath the apical membrane suggests that Otop1 may function in intracellular vesicles near the apical membrane. This characteristic of Otop1 would be ideal for the regulation of extracellular calcium levels. Interestingly, other major tissues that express Otop1 include the lactating mammary gland (data not shown), where regulation and transport of calcium is critical. Future studies will address whether the function of Otop1 to regulate purinergic signaling, and both extracellular and intracellular calcium levels, underlies development and function of otoconia and/or mammary gland function.

Acknowledgments

We thank C. Smith for technical help. This work was funded by NIH grants DC02236 (D.M.O.), NS032636 and NS036265 (M.P.G.), DC008603 (Y.W.L.), Neuroscience Blueprint Core grant (P30 NS057105), Bakewell Family Science Foundation, Microscopy and Digital Imaging (MDI) Core (P30 DC004665) and the Ornitz family charitable trust.

Abbreviations

Otopetrin 1	Otop1
Tilted	tlt
Mergulhador	mlh
Otopetrin domain	OD
transmembrane domain	TM
intracellular calcium concentration	$[Ca^{2+}]_i$
Zona Occluden-1	ZO-1

6. References

Burnstock G. Purine and pyrimidine receptors. Cell. Mol. Life Sci 2007;64:1471–1483. [PubMed: 17375261]

Carlstrom D, Engstrom H, Hjorth S. Electron microscopic and x-ray diffraction studies of statoconia. Laryngoscope 1953;63:1052–1057. [PubMed: 13110207]

Dobson CM. Protein folding and misfolding. Nature 2003;426:884–890. [PubMed: 14685248]

Grant W, Best W. Otolith-organ mechanics: lumped parameter model and dynamic response. Aviat. Space Environ. Med 1987;58:970–976. [PubMed: 3314853]

Hughes I, Binkley J, Hurle B, Green ED, NISC Comparative Sequencing Program. Sidow A, Ornitz DM. Identification of the Otopetrin Domain, a conserved domain in vertebrate otopetrins and invertebrate otopetrin-like family members. BMC Evolutionary Biology 2008;8:41. [PubMed: 18254951]

Hughes I, Saito M, Schlesinger PH, Ornitz DM. Otopetrin1 activation by purinergic nucleotides regulates intracellular calcium. Proc Natl Acad Sci U S A 2007;104:12023–12028. [PubMed: 17606897]

Hurle B, Ignatova E, Massironi SM, Mashimo T, Rios X, Thalmann I, Thalmann R, Ornitz DM. Non-syndromic vestibular disorder with otoconial agenesis in tilted/mergulhador mice caused by mutations in otopetrin 1. Hum Mol Genet 2003;12:777–789. [PubMed: 12651873]

Kim E, Hyrc KL, Speck J, Lundberg YW, Salles FT, Kachar B, Goldberg MP, Warchol ME, Ornitz DM. Regulation of cellular calcium in vestibular supporting cells by Otopetrin 1. J. Neurophysiol. 2010 in press.

Lane P. Tilted (tlt). Mouse News Lett 1986;75:28.

Mann S, Parker SB, Ross MD, Skarnulis AJ, Williams RJ. The ultrastructure of the calcium carbonate balance organs of the inner ear: an ultra-high resolution electron microscopy study. Proc. R. Soc. Lond. B. Biol. Sci 1983;218:415–424. [PubMed: 6136976]

Massironi SM, Dagli ML, Lima MR, Alvarez JM, Kipnis TL. A new mutant hairless mouse with lymph node hyperplasia and late onset of autoimmune pathology. Braz. J. Med. Biol. Res 1994;27:2401–2405. [PubMed: 7640630]

North RA. Molecular physiology of P2X receptors. Physiol. Rev 2002;82:1013–1067. [PubMed: 12270951]

Ornitz DM, Bohne BA, Thalmann I, Harding GW, Thalmann R. Otoconial agenesis in *tilted* mutant mice. Hearing Res 1998;122:60–70.

Suzuki H, Ikeda K, Furukawa M, Takasaka T. P2 purinoceptor of the globular substance in the otoconial membrane of the guinea pig inner ear. Am. J. Physiol 1997;273:C1533–1540. [PubMed: 9374638]

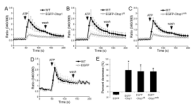

Fig. 1.

Change in intracellular Ca^{2+} levels ($[Ca^{2+}]_i$) in COS7 cells expressing *EGFP-Otop1*, *EGFP-Otop1^{tlt}*, and *EGFP-Otop1^{mlh}* in response to ATP. Untransfected cells are shown in black line with circle symbols and transfected cells are shown in gray line with open triangle symbols. (A) Untransfected wild type (n=181) cells showed a biphasic response to 100 μM ATP with an initial peak followed by a plateau phase which persisted until removal of the agonist (wash). The initial peak (rise) in $[Ca^{2+}]_i$ was much lower in the presence of *EGFP-Otop1* (n=161) where a sharp peak was absent. (B) *EGFP-Otop1^{tlt}*-positive cells (n=190) showed a reduced initial rise in $[Ca^{2+}]$ compared to the wild type (n=163) cells. (C) *EGFP-Otop1^{mlh}*-positive cells (n=202) showed a reduced initial rise in $[Ca^{2+}]_i$ compared to the wild type cells (n=220). (D) Transfection of EGFP (n=7) does not alter how COS7 cells respond to ATP (wild type cells: n=14). (E) Comparison of percent decrease of the initial peak values between untransfected and transfected cells. The percent decrease in cells transfected with *EGFP-Otop1*, *EGFP-Otop1^{tlt}*, *EGFP-Otop1^{mlh}* is significantly higher than those transfected with EGFP alone. * $p < 0.0001$ compared to EGFP control by two tailed student t-test. The graphs show average values ± standard deviation.

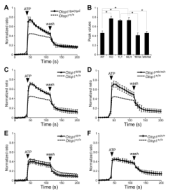

Fig. 2.

Otop1^{tlt} and *Otop1*^{mlh} macular cultures are unable to inhibit P2Y receptor function. (A) In response to 100 μM ATP, *Otop1*$^{+/+}$ cultures (n=6 dishes, each dish containing approximately 30 regions that were imaged) show a sustained increase in $[Ca^{2+}]_i$ with curve shape resembling a plateau until wash. This curve is also plotted as a dotted line in panels (C) through (F). *Otop1*$^{\beta gal/\beta gal}$ cultures (n=4) show a much higher peak followed by a plateau until wash. (B) Comparison of peak values. * $p < 0.0001$ by two-tailed student t-test. The graphs show average values ± standard deviation. (C, D) The response of *Otop1*$^{tlt/tlt}$ (n=7) and *Otop1*$^{mlh/mlh}$ (n=13) resembles that shown in *Otop1*$^{\beta gal/\beta gal}$ cultures (A). (E, F) The utricular epithelial cultures from heterozygous *tlt* (n=3) and *mlh* (n=3) mice respond like *Otop1*$^{+/+}$ cultures, showing an almost perfect match with the *Otop1*$^{+/+}$ curve.

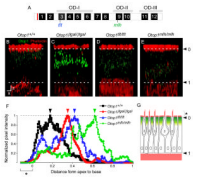

Fig. 3.

Apical localization of endogenous Otop1 is affected in *Otop1*^{tlt} and *Otop1*^{mlh} utricular maculae. (A) Schematic diagram showing the location of *tlt* and *mlh* mutations with respect to the 12 putative transmembrane (TM) domains of Otop1. *Tlt* and *mlh* are present within TM3 and TM9, which are parts of Otopetrin Domain I and II, respectively. The epitope (red line) for the anti-Otop1 antibody is located N-terminal to the putative TM domains. (B-E) Three-dimensional images were compressed in the y-axis to show the XZ plane of the macular epithelium. Phalloidin, shown in red, stains actin at the apical and basal ends of the sensory epithelium, which include the stereocilia bundles (hair cells), microvilli (supporting cells), apical membrane, and basal membrane. Otop1 signals are shown in green. White dashed lines indicate where '0' (arrowhead) and '1' (arrowhead) was assigned for the plot analysis in panel F. X- and Z-axis scale bars indicate 20 and 5 μm, respectively. On average, 150 μm of tissues were compressed to make XY plane stacked images. Representative images of 19 (*Otop1*+/+), 16 (*Otop1*$^{\beta gal/\beta gal}$), 10 (*Otop1*$^{tlt/tlt}$), and 12 (*Otop1*$^{mlh/mlh}$) samples are shown. (B) Wild type Otop1 is localized near the apex of the epithelium. (C) In *Otop1*$^{\beta gal/\beta gal}$ tissue, the β-galactosidase fusion protein is mis-localized and forms aggregates. (D, E) Otop1^{Tlt} and Otop1^{Mlh} are primarily localized in the mid to basal end of the epithelium. (F) Quantification of Otop1 signal intensities (y-axis; shown in B-E) with respect to the apical and basal end of the sensory epithelium. X-axis depicts distance from the apical to basal end, where '0' indicates a plane right above the apical membrane, where the lower end of stereocilia and microvilli are present. '1' represents where the basal membrane begins. The bracket with '*' indicates regions corresponding to stereocilia and microvilli. Each point was divided by the highest pixel value of each graph to obtain "normalized pixel intensity". Arrows indicate where the highest intensity values are found for each genotype. (G) Schematic diagram showing the apical expression of Otop1 in the macular epithelium.

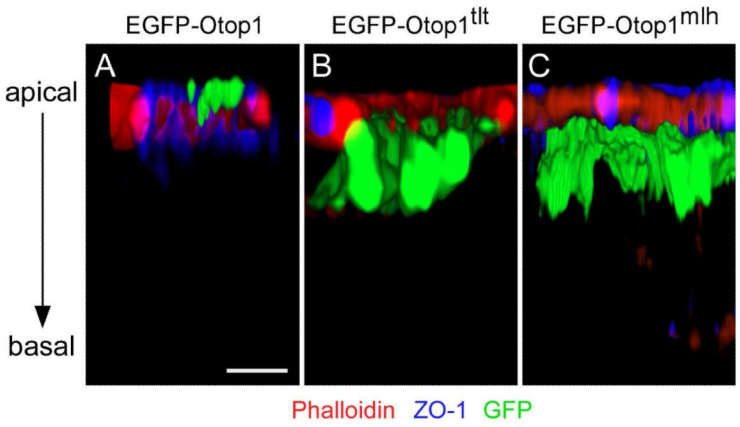

Fig. 4.

3D re-construction of rat utricular macular epithelia transfected with *EGFP-Otop1*, *EGFP-Otop1*^{tlt}, and *EGFP-Otop1*^{mlh}. After transfection, cultures were stained with anti-ZO-1 antibody (blue) and phalloidin (red) to mark the apical end of the epithelium. This is a representative figure of 15 images for each genotype. (A) EGFP-Otop1 is found in the most apical region, comparable to where ZO-1 is found. GFP is also present in the apical microvilli. Scale bar indicates 3 μm. (B) EGFP-Otop1^{Tlt} protein is present throughout the apical half of the sensory epithelial cell and the EGFP signal is not seen in the microvilli. (C) EGFP-Otop1^{Mlh} protein is localized in the supporting cell body and is excluded from the apical region.